

Prediction-Free Coordinated Dispatch of Microgrid: A Data-Driven Online Optimization Approach

Kaidi Huang, *Student Member, IEEE*, Lin Cheng, *Senior Member, IEEE*, Ning Qi, *Member, IEEE*,
David Wenzhong Gao, *Fellow, IEEE*,

Abstract—The integration of renewable energy sources (RES) into microgrids poses challenges to reliable and economic operation due to the inherent uncertainty and volatility of RES. Contrary to the previous dispatch methods that require precise predictions of RES, this paper proposes a novel prediction-free and data-driven coordinated dispatch framework for reliable microgrid operations. In the offline stage, ex-post optimal dispatch sequences are generated based on historical dispatch from "God's-eye view". The sequences offer a global reference and are sequentially updated based on the newly observed data. Subsequently, we propose an adaptive virtual-queue-based online convex optimization (OCO) method to generate the real-time control policy of microgrid, which aim to minimize the instant operation cost while tracking the offline reference. We provide theoretical proof that the proposed method outperforms the existing OCO methods and admits sublinear dynamic regret bound and sublinear hard cumulative constraint violation bound for OCO with time-varying constraints. Case study illustrates that the proposed method outperforms state-of-the-art methods in terms of economic optimality, computational efficiency, and security.

Index Terms—Microgrid, online optimization, energy storage, coordinated dispatch, data-driven method.

I. INTRODUCTION

MICROGRID (MG) will be an essential part of the future power grid, as it enables the integration and coordination of distributed renewable energy sources (RES), energy storage (ES), distributed generators (DGs), and loads. This paper focuses on ensuring reliable and economic dispatch of MG under strong uncertainties of RES.

Early research mainly focused on the day-ahead dispatch of MG, and several approaches are commonly used to handle uncertainty, including robust optimization (RO), stochastic optimization (SO), and chance-constrained optimization (CCO) [1]–[3]. RO addresses uncertainty by finding solutions that perform reliably across a predefined range of uncertainties, ensuring stability even under worst-case scenarios. In contrast, SO incorporates the probabilistic distribution of uncertainties into the decision-making process, aiming to optimize expected outcomes and offering solutions that are statistically optimized. However, the day-ahead strategy will encounter optimality and feasibility issues in the practical real-time operation due to the non-anticipativity. This motivates the research on the multi-period coordinated dispatch and real-time operation of MG [4]–[7]. Ref. [5] illustrates the implementation of

economic model predictive control (EMPC) methods of MG and aims to find the optimal operation. Ref. [6] explores the multi-stage real-time stochastic operation using a hybrid model predictive control (MPC) and approximate dynamic programming approach, which achieves sufficiently good real-time operational solutions through continuously updated forecast. Ref. [7] develops a two-stage coordinated operation model via deep reinforcement learning, enhancing efficiency and adaptability to RES variations based on hourly predicted data.

However, the existing research faces two key limitations: (i) The complexity and inaccuracy of mathematical modeling for uncertainties. The interval-based fluctuations assumed by RO and the probabilistic distributions used in SO may not accurately reflect the highly volatile nature of RES in MG. (ii) Due to the limited capacity, lacking of meteorological measuring devices and numerical weather predictions [8], [9], the precise predictions of RES are practically unavailable or unreliable in MG. Therefore, existing approaches that highly-dependent on predictions are still not effectively applicable in MG. It is imperative to explore approaches less reliant on predictions and have fast response speed.

Lyapunov optimization and online convex optimization (OCO) are both optimization techniques for online decision-making in uncertain environments, without the need for prediction. Lyapunov uses a "1-lookahead" pattern, solving the drift problem after observing uncertainty. In contrast, OCO employs a "0-lookahead" pattern, making decisions before observing uncertainty [10]. Due to rapid fluctuations of RES and measurement delays, OCO is more applicable in energy management of MG. As volatility and uncertainty increase, OCO has gained wider attention in power system [11]–[13]. Ref. [11] proposes an OCO-based algorithm for dynamically setting electricity prices to promote optimal usage and stabilize load curves. In [12], a distributed control strategy based on OCO is proposed for coordinating multiple energy storages (ESs) to enhance frequency regulation, offering more accurate control than current prediction-based algorithms. In [13], an OCO-based algorithm is developed for real-time management of building energy systems to enhance their contribution to grid ancillary services under uncertainties and limited information. To the best of our knowledge, no research work has yet developed an OCO-based algorithm for the dispatch of MG.

OCO focused on the problem (1), the convex objective function f_t and constraint g_t are unknown before x_t is determined by OCO algorithm. OCO algorithms are problem-dependent without a unified paradigm, which all focus on the performance estimation with metrics like Reg, Vio [10].

The first metric *regret* is shown in (2), quantifying the suboptimality. Depending on different baselines y_T , regret is di-

Kaidi Huang and Lin Cheng are with the Department of Electrical Engineering, Tsinghua University, Beijing 100084, China (e-mail: hjd23@mails.tsinghua.edu.cn). Ning Qi is with the Department of Earth and Environmental Engineering, Columbia University. David Wenzhong Gao is with Department of Electrical and Computer Engineering, University of Denver, CO 80210 USA.

TABLE I
COMPARING OF THIS PAPER TO RELATED WORKS ON ONLINE CONVEX OPTIMIZATION

Reference	Constraint type	Regret benchmark	Regret bound	Constraint violation	Constraint violation bound
[14]	Time-varying	Dynamic	$O(\max(T^\delta P_x, T^{1-\delta}))$	Vio^{soft}	$O(T^{1-\delta/2})$
[15]	Time-invariant	Static	$O(\sqrt{T})$	Vio^{soft}	$O(1)$
[16]	Time-varying	Dynamic	$O(\sqrt{TP_x})$	Vio^{soft}	$O(\max(T^{3/4}, P_g))$
[17]	Time-invariant	Dynamic	$O(\sqrt{T(1+P_x)})$	Vio^{hard}	$O(\sqrt{T})$
[18]	Time-varying	Static	$O(\sqrt{T})$	Vio^{soft}	$O(T^{3/4})$
[19]	Time-varying	Static	$O(T^{\max\{1-a-c, c\}})$	Vio^{hard}	$T^{1/2-c/2}$
[20]	Time-varying	Static	$O(T^{\max\{\delta, 1-\delta\}})$	Vio^{hard}	$O(T^{1-\delta/2})$
This paper	Time-varying	Dynamic	$O(T^{1/2+\chi}\sqrt{1+P_x})$	Vio^{hard}	$O(\log_2(T)T^{1-\chi/2})$

vided into: *static regret* with $\mathbf{y}_T = (x^*, \dots, x^*)$ which is a single best action; *dynamic regret* with $\mathbf{y}_T = (x_1^*, \dots, x_T^*)$ which is the global optimal solution. The second metric ***cumulative constraint violation*** is shown in (3a), quantifying the safety performance. However, this metric tolerates constraint violations as long as they are compensated by strictly feasible decisions. We consequently adopt a stricter metric as shown in (3b) [17]. We call it *hard cumulative constraint violation*. The literature generally agrees that an OCO algorithm performs well if its regret and constraint violation are sublinear function of T . This implies that in the time-average sense, the performance of the algorithm is no worse than that of the global optimal solution.

$$\min_{x_t \in X} \sum_{t=1}^T f_t(x_t) \text{ s.t. } g_t(x_t) \leq 0, t=1,2,\dots,T \quad (1)$$

$$\text{Reg}(\mathbf{x}_T, \mathbf{y}_T) := \sum_{t=1}^T f_t(x_t) - \sum_{t=1}^T f_t(y_t) \quad (2)$$

$$\text{Vio}^{\text{soft}} := \left\| \left[\sum_{t=1}^T g_t(x_t) \right]_+ \right\| \quad (3a)$$

$$\text{Vio}^{\text{hard}} := \sum_{t=1}^T \| [g_t(x_t)]_+ \| \quad (3b)$$

Clearly, dynamic regret and hard cumulative constraint violation are more suitable for performance guarantee in MG with strong volatility. However, a crucial challenge is to achieve sublinear dynamic regret and hard cumulative constraint violation bound simultaneously under only common assumptions, which has not yet been addressed in existing research.

To fill in the research gap in both methodology and algorithm, the main contributions of this paper are threefold:

1) **Dispatch Methodology.** A novel data-driven, two-stage coordinated dispatch framework is proposed for MG, obviating the need for prediction and complex uncertainty modeling. We introduce generic energy storage (GES) to uniformly model dispatchable resources. In offline stage, ex-post optimal dispatch sequences are generated based on historical data. In online stage, a “reference” with global vision is sequentially updated based on these sequences and newly observed data. The real-time control actions, generated from OCO algorithm, aim to minimize the operating cost while tracking the reference.

2) **Solution Algorithm.** We propose a novel adaptive virtual-queue-based (VQB) online optimization algorithm based on the OCO framework. The proposed algorithm surpasses existing OCO algorithms in both suboptimality and safety metrics. To the best of our knowledge, we are the first to achieve and prove sublinear dynamic regret bound and sublinear hard cumulative constraint violation bound for OCO with time-varying constraints. A summary of the comparison between this paper and related works is presented in Table I.

3) **Numerical Study.** We validate the proposed method using ground-truth 5-minute-interval data over 68 continuous days. Case study shows that our method outperforms previous approaches in terms of economy, security, and computational efficiency due to (1) the strong performance guarantee of the designed algorithm, (2) the global vision provided by the reference. We analyzed the ability of the proposed method to maintain stable operation over long time scale and the impact of communication limitations on operational effectiveness.

The remainder of the paper is organized as follows. The MG structure and its operating model are formulated in Section II. The data-driven, two-stage coordinated dispatch framework and the adaptive VQB online optimization algorithm for MG are developed in Section III. Numerical study based on real-world data is provided in Section IV. Finally, conclusions are summarized in Section V.

II. PROBLEM FORMULATION

A typical MG consists of RES, distributed generator (DG), ES, flexible load, conventional load, etc, and can be connected to the main grid via tie-line. Most of flexible loads, such as thermostatically controlled load and electric vehicle, have the attributes of ES, hence motivating the concept of “virtual energy storage” (VES) [21]. ES and VES can be considered under a common framework called GES to unify modeling. The model transformation from physical load to GES can be referenced in [3]. The dispatch model is given below.

Considering a daily operation horizon with a 5-minute time interval, the index of periods is $t \in \Omega_T = \{1, 2, \dots, T\}$. The objective function is given in (4a), which is to minimize the MG operation cost while smoothing the tie-line power. The MG operation cost includes the incentive cost of GESs (4b), the cost of grid power (4c), and the generation cost of

DGs (4d). Eq. (4e) represents the penalty term for smoothing the tie-line power. The power intermittence of RES will lead to considerable power fluctuations to the MG, which may further threaten the secure operation of the main grid through tie-line, so it is important to suppress tie-line power fluctuations to reduce the impact on the main grid [22].

Constraints (5)-(6) are the output limit and ramp constraint for DG. Constraints (7)-(8) limit the charge/discharge power of GES. Since sufficient conditions are satisfied (i.e., charging price is lower than discharging price), the complementary constraint for charging and discharging is relaxed and has been removed from model [23]. Constraint (9) defines the relationship among charge power, discharge power, SoC, and additional energy input from baseline consumption. Constraint (10) represents time-varying upper and lower bounds on SoC. The time-varying and stochastic power limit and SOC limit of GES can be obtained by data-driven methods (i.e., load decomposition and parameter identification) [24]. Chance constraints (8) and (10) can adopt different confidence levels for different reliability preferences [25]. Constraint (11) ensures a sustainable energy state for the GES overtime. Constraints (12)-(15) are power flow for radial MG which can be modelled with the *DistFlow* model [4].

Objective function:

$$\min \sum_{t \in \Omega_T} \left(C_t^{\text{GES}} + C_t^{\text{grid}} + C_t^{\text{DG}} \right) + C^{\text{pl}} \quad (4a)$$

$$C_t^{\text{GES}} = \sum_{j \in \Omega_G} (c_{d,j,t}^{\text{GES}} P_{d,j,t} + c_{c,j,t}^{\text{GES}} P_{c,j,t}) \Delta t \quad (4b)$$

$$C_t^{\text{grid}} = \lambda_t P_t^{\text{grid}} \Delta t \quad (4c)$$

$$C_t^{\text{DG}} = \sum_{k \in \Omega_D} (a_k (P_{k,t}^{\text{DG}})^2 + b_k P_{k,t}^{\text{DG}} + c_k) \Delta t \quad (4d)$$

$$C^{\text{pl}} = \sum_{t \in \Omega_T} c^{\text{pl1}} (P_t^{\text{grid}} - P_{t-1}^{\text{grid}})^2 + c^{\text{pl2}} (P_t^{\text{grid}} - \bar{P}^{\text{grid}})^2 \quad (4e)$$

Constraints: $\forall t \in \Omega_T, \forall k \in \Omega_D, \forall j \in \Omega_G, \forall m \in \Omega_B$

$$\underline{P}_k^{\text{DG}} \leq P_{k,t}^{\text{DG}} \leq \bar{P}_k^{\text{DG}} \quad (5)$$

$$-P_{k,\text{RD}}^{\text{DG}} \leq P_{k,t+1}^{\text{DG}} - P_{k,t}^{\text{DG}} \leq P_{k,\text{RU}}^{\text{DG}} \quad (6)$$

$$0 \leq P_{c,j,t}^{\text{GES}}, \quad 0 \leq P_{d,j,t}^{\text{GES}} \quad (7)$$

$$\mathbb{P} \left(P_{c,j,t}^{\text{GES}} \leq \bar{P}_{c,j,t}^{\text{GES}} \right) \geq 1 - \varepsilon, \quad \mathbb{P} \left(P_{d,j,t}^{\text{GES}} \leq \bar{P}_{d,j,t}^{\text{GES}} \right) \geq 1 - \varepsilon \quad (8)$$

$$\text{SoC}_{j,t+1}^{\text{GES}} = (1 - \mathcal{E}_j^{\text{GES}}) \text{SoC}_{j,t}^{\text{GES}} + \eta_{c,j} P_{c,j,t}^{\text{GES}} \Delta t / S_j^{\text{GES}} - P_{d,j,t}^{\text{GES}} \Delta t / (\eta_{d,j} S_j^{\text{GES}}) + \pi_{j,t}^{\text{GES}} \quad (9)$$

$$\mathbb{P} \left(\text{SoC}_{j,t}^{\text{GES}} \leq \text{SoC}_{j,t}^{\text{GES}} \leq \overline{\text{SoC}}_{j,t}^{\text{GES}} \right) \geq 1 - \varepsilon \quad (10)$$

$$\text{SoC}_{j,T}^{\text{GES}} = \text{SoC}_{j,0}^{\text{GES}} \quad (11)$$

$$P_{b+1,t}^{\text{PF}} = P_{b,t}^{\text{PF}} - P_{b+1,0,t}^{\text{PF}} - P_{m,t}^{\text{L}} + P_{m,t}^{\text{R}} + P_{d,m,t}^{\text{GES}} - P_{c,m,t}^{\text{GES}}, b \in Br(m) \quad (12)$$

$$Q_{b+1,t}^{\text{PF}} = Q_{b,t}^{\text{PF}} - Q_{b+1,0,t}^{\text{PF}} - Q_{m,t}^{\text{L}} + Q_{d,m,t}^{\text{GES}} - Q_{c,m,t}^{\text{GES}}, b \in Br(m) \quad (13)$$

$$V_{m+1,t}^{\text{BUS}} = V_{m,t}^{\text{BUS}} - (R_b P_{b,t}^{\text{PF}} + X_b Q_{b,t}^{\text{PF}}) / V^{\text{S}}, b \in Br(m, m+1) \quad (14)$$

$$\underline{V}^{\text{BUS}} \leq V_{m,t}^{\text{BUS}} \leq 1 + \bar{V}^{\text{BUS}} \quad (15)$$

where Ω_G , Ω_D and Ω_B are the sets of GES assets, DG assets and buses, respectively. $c_{d,j,t}^{\text{GES}}$, $c_{c,j,t}^{\text{GES}}$ are the operational costs of GES asset j . $P_{d,j,t}$, $P_{c,j,t}$ are the discharge and charge power of GES asset j . Δt is the unit dispatch interval. The time of use (ToU) price is given by λ_t . P_t^{grid} is the power bought from the main grid. $P_{k,t}^{\text{DG}}$ is the power output of DG. a_k , b_k , c_k are cost coefficients of DG. \bar{P}^{grid} is the average tie-line power over the entire dispatch cycle. c^{pl1} and c^{pl2} are constant coefficients. Up and down ramp rate for $P_{k,t}^{\text{DG}}$ are given by $P_{k,\text{RU}}^{\text{DG}}$ and $P_{k,\text{RD}}^{\text{DG}}$. Underline and overline denote minimum and maximum. ε is the probability level of chance constraints. $\mathcal{E}_j^{\text{GES}}$, $\eta_{c/d,j}$, S_j^{GES} and $\pi_{j,t}^{\text{GES}}$ define the self-discharge rate, charge/discharge efficiency, capacity, and baseline consumption item. b , m are the index of branches and buses, $Br(m)$ is the set of branches that connect to bus m , $Br(m,l)$ is the set of the branch between bus m and l , $P_{b,t}^{\text{PF}}$, $Q_{b,t}^{\text{PF}}$ are the active and reactive power that flows on branch b , $P_{b,0,t}^{\text{PF}}$, $Q_{b,0,t}^{\text{PF}}$ are the active and reactive power that flows on the lateral branch. We set the GES to have a fixed power factor. $P_{m,t}^{\text{L}}$, $P_{m,t}^{\text{R}}$ are the power of load and RES. $V_{m,t}^{\text{BUS}}$ is the voltage of bus m , V^{S} is voltage of the substation bus, R_b , X_b is the resistance and reactance of branch b .

III. DATA-DRIVEN TWO-STAGE COORDINATED DISPATCH OF MG BASED ON OCO

Solving the proposed dispatch model will yield the optimal operation strategy, but it is not practical due to two main reasons: (i) the uncertainty of the power limit and SOC limit of GES, which are time-varying and stochastic, makes chance constraints (8) and (10) intractable, and (ii) the nonanticipativity of RES and load can lead to poor performance of the operation strategy derived from the proposed dispatch model.

In this paper, we employ a deterministic reformulation and make the chance constraints tractable. We model the dispatch of MG as an online decision-making problem, where uncertainty is continually revealed during real-time operation. We develop an adaptive VQB online optimization algorithm that utilizes the latest uncertainty information for real-time control.

To avoid myopic decision-making resulting from the lack of predictions and the time-coupling characteristics of GES, we propose a two-stage coordinated approach as illustrated in Fig. 1: We devise an empirical reference to provide a global vision in the offline stage; The reference is sequentially updated in the online stage. The real-time control actions, generated from the proposed OCO algorithm, aim to minimize the instant operating cost while tracking the reference.

A. Offline Stage: Empirical Learning

Chance constraints (8) and (10) allow for a deterministic and tractable reformulation [3]. We employ the standard reformulation from [26], and yields:

$$P_{c,j,t}^{\text{GES}} \leq \mu_{\bar{P}_{c,j,t}^{\text{GES}}} - F_{\bar{P}_{c,j,t}^{\text{GES}}}^{-1}(1 - \varepsilon) \sigma_{\bar{P}_{c,j,t}^{\text{GES}}} \quad (16a)$$

$$P_{d,j,t}^{\text{GES}} \leq \mu_{\bar{P}_{d,j,t}^{\text{GES}}} - F_{\bar{P}_{d,j,t}^{\text{GES}}}^{-1}(1 - \varepsilon) \sigma_{\bar{P}_{d,j,t}^{\text{GES}}} \quad (16b)$$

$$\text{SoC}_{j,t}^{\text{GES}} \leq \mu_{\overline{\text{SoC}}_{j,t}^{\text{GES}}} - F_{\overline{\text{SoC}}_{j,t}^{\text{GES}}}^{-1}(1 - \varepsilon) \sigma_{\overline{\text{SoC}}_{j,t}^{\text{GES}}} \quad (16c)$$

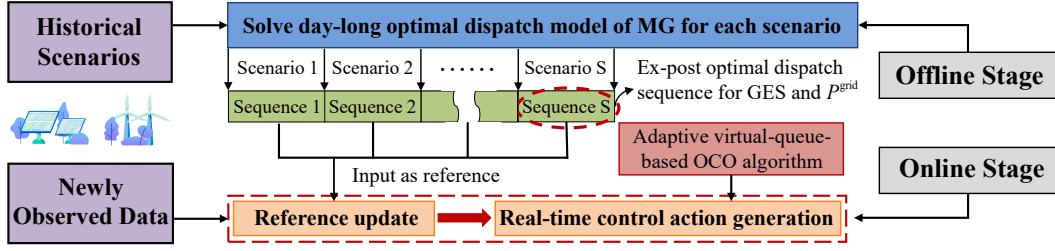


Fig. 1. Data-driven two-stage coordinated dispatch framework.

$$SOC_{j,t}^{GES} \leq \mu_{SOC_{j,t}^{GES}} - F^{-1}_{SOC_{j,t}^{GES}}(1-\varepsilon)\sigma_{SOC_{j,t}^{GES}} \quad (16d)$$

where normalized inverse cumulative distribution function F^{-1} can be obtained by Monte Carlo sampling of any kind of distribution (e.g., normal distribution, beta distribution) [27]. μ , σ are the mean and standard deviation of the distribution. Thus, the dispatch model becomes convex programming and can be efficiently solved by commercial solvers.

Compared to predictions, historical data are much more accessible. We can fully leverage the value of historical data to provide dispatch experience for online operation. Specifically, a collection of historical scenarios is utilized, denoted by:

$$\{\ell_{t,s}^R, \ell_{t,s}^L\}_{t=1}^T, s \in \{1, 2, \dots, S\}, \quad (17)$$

where ℓ_t^R and ℓ_t^L are RES power and load in period t , S is the number of historical scenarios. For each scenario, we solve the day-long optimal dispatch model of MG:

$$\begin{aligned} & \min \text{objective function (4)} \\ & \text{s.t. constraints (5)-(7),(9),(11)-(16).} \end{aligned} \quad (18)$$

Then, we get S ex-post optimal SOC sequences for GES: $R_s^{SOC} = \{R_{t,s}^{SOC}\}_{t=1}^T$. Due to the time-coupling characteristics of GES, these sequences will provide reference for real-time operation. Similarly, the peak shaving and valley filling of tie-line power also exhibit time-coupling characteristics. Therefore, we also store the S ex-post optimal P^{grid} sequences for tie-line power: $R_s^{\text{grid}} = \{R_{t,s}^{\text{grid}}\}_{t=1}^T$.

B. Online Stage: Real-Time Control Policy

(a) Reference update

In the online stage, real-time control actions are generated every 5 minutes, with the reference being determined beforehand. Reference leverages historical experience to avoid myopic decisions in real-time operations, thus providing a global vision. The core idea of data-driven reference update is that if the uncertainty realization observed in the operating day is closer to a particular historical scenario, then the optimal dispatch sequence of the scenario should be assigned with a larger weight coefficient in the reference.

Specifically, define vector $\ell_{[t]}$ to represent the uncertainty observed in the real-time operation from the beginning of the operating day to the current period t :

$$\ell_{[t]} = [\ell_1^N, \ell_1^P, \dots, \ell_t^N, \ell_t^P]. \quad (19)$$

Define $\ell_{[t],s}$ that corresponds to the s th historical scenario:

$$\ell_{[t],s} = [\ell_{1,s}^N, \ell_{1,s}^P, \dots, \ell_{t,s}^N, \ell_{t,s}^P]. \quad (20)$$

Consequently, the similarity between $\ell_{[t]}$ and $\ell_{[t],s}$ can be measured by the Euclidean distance as $\|\ell_{[t]} - \ell_{[t],s}\|_2$. Then, we can determine and sequentially update the reference by taking the weighted average of those ex-post optimal sequences. Let $R_t^{\text{SOC,ref}}$, $R_t^{\text{grid,ref}}$ be the reference in period t , with the update policy defined as:

$$R_t^{\text{SOC,ref}} = \sum_{s=1}^S \omega_t^s R_{t,s}^{\text{SOC}}, R_t^{\text{grid,ref}} = \sum_{s=1}^S \omega_t^s R_{t,s}^{\text{grid}}, \quad (21)$$

where ω_t^s is the weight of historical scenario s , reflecting the similarity between the operating day and the s th historical scenario. ω_t^s in period t is calculated using Nadaraya-Waston kernel regression technique [28]:

$$\omega_t^s = \frac{K_t(\ell_{[t]}, \ell_{[t],s})}{\sum_{s'=1}^S [K_t(\ell_{[t]}, \ell_{[t],s'})]}, \text{ where } K_t(x, y) = e^{-\frac{(\|x-y\|_2)^2}{t\tau}}. \quad (22)$$

where $K_t(x, y)$ is defined as the Gaussian kernel function; τ is the bandwidth parameter. We have $\sum_s \omega_t^s = 1$, and scenarios more similar to the current day are assigned larger weight. Thus, $\{\omega_t^s\}_{s=1}^S$ can be viewed as a discrete probability distribution, and the reference can be viewed as the conditional expectation of S ex-post optimal sequences over the operating day. The reference is updated every 5 minutes, which is a sequential process along with time. Reference update leverages the latest information revealed in the real-time operation, providing a globally informed benchmark for the real-time control action generation.

(b) Real-time control action generation—OCO algorithm

After reference update, the real-time control actions aim to minimize the instant operating cost while tracking the reference. Therefore, the online decision optimization problem in period t can be formulated as:

$$\begin{aligned} \min f_t = & C_t^{\text{GES}} + C_t^{\text{grid}} + C_t^{\text{DG}} + \varphi_1 (\text{SOC}_t^{\text{GES}} - R_t^{\text{SOC,ref}})^2 \\ & + \varphi_2 (P_t^{\text{grid}} - R_t^{\text{grid,ref}})^2 \end{aligned} \quad (23)$$

s.t. constraints (5)–(7),(9),(12)–(16).

The second part in the objective represents the penalty for deviation from the reference, where φ_1 , φ_2 are weight coefficients. Constraint (11) is excluded, as (23) is local optimization, unsuitable for addressing inter-temporal constraints. However, appropriately tracking the reference can still ensure a sustainable energy state for the GES overtime.

Due to communication limitations and control delay, especially in MGs spanning large areas or with poor communication conditions, the uncertainty observed during

Algorithm 1 : Data-driven adaptive VQB OCO Algorithm

[Offline Stage For Empirical Learning]
Input: Historical scenarios of RES and load:

$$\{\ell_{t,s}^R, \ell_{t,s}^L\}_{t=1, s \in \{1, 2, \dots, S\}}^T.$$

For $s = 1, \dots, S$

Solve the day-long optimal model (18).

 Store the optimal solution R_s^{SOC} and R_s^{grid} .

end
[Online Stage For Real-Time Control]
Step 1 - Initialization:

 Set $Q_i(0) = 0$, $x_{i,1} \in X$, $x_1 = \sum_{i=1}^N \rho_{i,1} x_{i,1}$,

$$\rho_{i,1} = (N+1)/[i(i+1)N], \forall i \in \{1, 2, \dots, N\}.$$

Step 2 - Iteration:
For $t = 2, \dots, T$

 Update reference $R_t^{\text{SOC,ref}}$ and $R_t^{\text{grid,ref}}$ using (21)-(22).

 Update Q_i for each expert in parallel using (26).

 Update $x_{i,t}$ for each expert in parallel using (25).

 Execute weighted average x_t calculated by (27).

 Observe $f_t(x_t)$ and $g_t(x_t)$.

Update the weight of each expert by (28).

end
Step 3 - Output: x_t , $f_t(x_t)$, $t = 1, \dots, T$, Reg, Vio.

real-time operation can be outdated by several minutes. This delay means that some constraints and the objective function in (23) cannot be modeled accurately in real-time, i.e., decision is made before the observation of the uncertainty. Sequential decision-making problems under this ‘‘0-lookahead’’ pattern are typically addressed through OCO [10].

Hereby, we develop a novel adaptive VQB OCO algorithm, which is a general-purpose algorithm designed for problem (1). The main theoretical results are explained in Theorem 1. To the best of our knowledge, we are the first to achieve and prove a sublinear dynamic regret bound and sublinear hard cumulative constraint violation bound for OCO with time-varying constraints. The algorithmic process is shown in Algorithm 1, including the offline stage and reference update. However, even without these components, the algorithm still possesses the properties outlined in Theorem 1.

It is worth noting that problem (23) can be formulated in the form of problem (1), where x_t refers to the discharge and charge power of GESs and the power output of DGs.

To delve into the rationale behind the algorithm, we commence the process with the Lagrange multiplier method:

$$x_t = \operatorname{argmin}_{x \in X} L_t(\lambda_t, x) = \operatorname{argmin}_{x \in X} \{f_t(x) + \langle \lambda_t, g_t(x) \rangle\}, \quad (24)$$

where λ_t is the dual variables and $\langle x, y \rangle$ denotes the standard inner product. In the online setting, we lack prior knowledge of f_t and g_t when making decision x_t . We estimate f_t using first-order Taylor expansion, and use the clipper constraint function $[g_{t-1}(x)]_+$ to replace $g_t(x)$. λ_t is substituted by virtual queue $Q(t-1)$ acting like a ‘‘queue backlog’’ of constraint violations. The regularization term $\|x - x_{t-1}\|^2$ is added to smooth the difference between coherent actions and enhance the stability

of the algorithm. With these adjustments, (24) can be transformed into its online counterpart:

$$x_t = \operatorname{argmin}_{x \in X} \{ \alpha_{t-1} \langle \partial f_{t-1}(x_{t-1}), x - x_{t-1} \rangle + \alpha_{t-1} \beta_{t-1} \langle Q(t-1), [g_{t-1}(x)]_+ \rangle + \|x - x_{t-1}\|^2 \}. \quad (25)$$

We update each element in the virtual queue with (26). The update strategy is that when violation occurs the violation is accumulated into virtual queue, and we use a round-dependent variable θ_{t-1} to guarantee a minimum value of virtual queue that prevent the algorithm from taking aggressive decisions which lead to large constraint violation.

$$Q^k(t-1) = \max(Q^k(t-2) + \beta_{t-1} [g_{t-1}^k(x_{t-1})]_+, \theta_{t-1}) \quad (26)$$

Then, the most critical issue is to determine the learning rate α_{t-1} for (25), one of the key parameters in optimization. A fixed learning rate may not adapt well to changes in the environment during online optimization. Inspired by [29], we use the expert tracking algorithm to address this dilemma. Our idea is to run multiple (25), i.e., experts, in parallel, each with a different learning rate α_{t-1} , and then a set of actions x_{t-1} are generated by all experts, finally we output the weighted average as (27). After observing the objective function f_t , the weights of each expert $\rho_{i,t}$ are updated according to their empirical performance on the data using an exponential weighting scheme, as shown in (28).

$$x_t = \sum_{i=1}^N \rho_{i,t} x_{i,t} \quad (27)$$

$$l_t(x_{i,t}) = \langle \partial f_t(x_t), x_{i,t} - x_t \rangle, \rho_{i,t+1} = \frac{\rho_{i,t} e^{-\gamma l_t(x_{i,t})}}{\sum_{i=1}^N \rho_{i,t} e^{-\gamma l_t(x_{i,t})}} \quad (28)$$

Based on the above analysis, we put forward Algorithm 1 and are ready to present the main result of the algorithm. First, we make the following assumptions on the objective function and constraint function, which are useful in later analysis. Notably, these assumptions align with standard practices in OCO literature and are applicable to the dispatch of MG.

Assumption 1. The function f_t and g_t are convex. The set X is convex and there is a positive constant $d(X)$ such that

$$\|x - y\| \leq d(X), \forall x, y \in X. \quad (29)$$

Assumption 2. There exists a positive constant F such that

$$|f_t(x) - f_t(y)| \leq F, \|g_t(x)\| \leq F, \forall t, \forall x, y \in X. \quad (30)$$

Assumption 3. The subgradients $\partial f_t(x)$ and $\partial g_t(x)$ exist. There exists a positive constant G such that

$$\|\partial f_t(x)\| \leq G, \|\partial g_t(x)\| \leq G, \forall t, \forall x, y \in X. \quad (31)$$

The regret and hard cumulative constraint violation bounds for Algorithm 1 are provided in the following theorem.

Theorem 1. Suppose Assumption 1-3 hold. For any $T \in \mathbb{N}_+$, if we choose appropriate N , γ , $\{\alpha_{i,t}\}$, $\{\beta_t\}$ and $\{\theta_t\}$:

$$N = \left\lceil \frac{1}{2} \log_2(1+T) \right\rceil + 1, \gamma = \frac{1}{\sqrt{T}}, \alpha_{i,t} = \frac{2^{i-1}}{t^{\frac{1}{2} + \chi}}, \quad (32)$$

$$\beta_t = t^{\frac{1}{2} + \delta}, \theta_{i,t} = 2^{i-1} t, \forall i \in \{1, 2, \dots, N\}, \frac{1}{2} > \delta > \chi > 0,$$

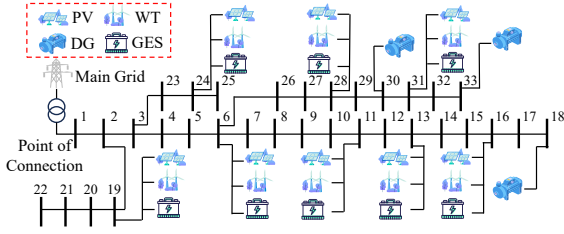


Fig. 2. 33-Bus radial MG diagram.

then Algorithm 1 achieves:

$$\text{dynamic regret} = O(T^{\frac{1}{2} + \chi} \sqrt{1 + P_x}), \quad (33)$$

$$\text{Vio}^{\text{hard}} = O(\log_2(T) T^{1 - \frac{\chi}{2}}), \quad (34)$$

where P_x is defined as:

$$P_x = \sum_{t=1}^{T-1} \|x_{t+1}^* - x_t^*\|. \quad (35)$$

Proof: The proof is given in Appendix.

IV. CASE STUDY

A. Set-up

The proposed method is tested on the IEEE 33 bus radial system, configured as a MG, illustrated in Fig. 2 [30]. The system is set up with ground-truth data from a MG in Jiangsu Province, China. The rated power of WTs, PVs, DGs, ESs, and VESs are 2.3MW, 1.3MW, 2.5MW, 1.4MW, and 0.7MW, with total loads sized around 5MW. The bus voltage limit is set as 1 ± 0.05 p. u. Stochastic variations for prices are set as 15% deviation from their forecasted value. The computing environment is Core i7-1165G7 @ 2.80GHz, 16GB RAM laptop. The whole problem is coded in MATLAB with YALMIP interface and solved by CPLEX 12.6.

B. Dispatch Results Compared With Different Methods

We introduce three indices to evaluate the operational performance of MG: operation cost, voltage satisfaction rate, and tie-line power fluctuation which is defined as:

$$\xi_1 = \frac{\sum_{t=1}^{T-1} |P_{t+1}^{\text{grid}} - P_t^{\text{grid}}|}{T-1}, \quad \xi_2 = \frac{\sum_{t=1}^T |P_t^{\text{grid}} - \bar{P}^{\text{grid}}|}{T} \quad (36)$$

To fully demonstrate the advantage of our method, we conducted optimization for 68 consecutive days based on the actual data, and compared the following methods:

- 1) **M1:** Scenario-based stochastic optimization [31].
 - 2) **M2:** EMPC [5], to the authors' best knowledge, is currently the state-of-the-art method. The key idea is rolling-horizon optimization, using a predictive model, cost function, and solvers. Short-term prediction of net load (including RES and load) are generated with the error (MAPE) set as 10%.
 - 4) **M3:** The proposed data-driven two-stage method.
 - 5) **M4:** Deterministic optimization with perfect knowledge.
- The dispatch results of M1-M4 over 68 days are compared in Table II. M2* is EMPC method with MAPE set as 20%. For ease of analysis, we use a typical scenario as an example,

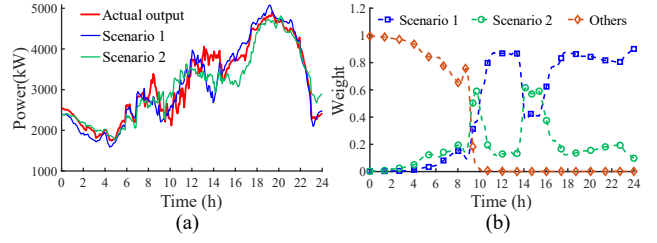


Fig. 3. (a) Net load and (b) historical scenarios weight variations of M3.

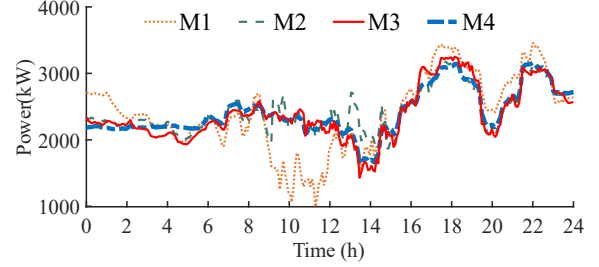


Fig. 4. Comparison of tie-line power between M1-M4.

as shown in Fig. 3. Figs. 4-8 detail the dispatch results of M1-M4 for the typical scenario. It can be found that:

- (1) In terms of average operation cost, M3 is closest to M4, differing by only 1.08%, with their tie-line power curves also closely aligned. This implies that the proposed data-driven two-stage method can nearly achieve the effect of the global optimal solution. M1 yields the worst result. Although day-ahead SO considers expected costs across multiple scenarios, it cannot handle intraday fluctuations of RES. These fluctuations, absorbed by external grid, cause significant power volatility and increased costs. We observed that the reference update of M3 is somewhat similar to prediction. Therefore, the main difference between the proposed M3 and EMPC lies in how they respond to rapid fluctuations of RES: During the peak price periods (12-15h), there was a sudden drop in the output of RES, as shown in Fig. 3(a). Based on real-time data, M3 mitigated the fluctuation of RES by increasing the output of DGs and enhancing the discharge power of GESs. Therefore, the rapid response enabled the tie-line power of M3 to exhibit a trend similar to that of M4, as shown in Fig. 6(c) and (d). In contrast, due to prediction errors, the sudden drop of RES was not anticipated. Consequently, EMPC did not respond in time, leading to a sudden increase in tie-line power and resulting in high purchase costs, as shown in Fig. 6(b). Therefore, M3 demonstrates a faster response speed and better robustness to the uncertainties of RES.

TABLE II
COMPARISONS OF POWER DISPATCH OVER 68 DAYS

Indices	M1	M2*	M2	M3	M4
Average operation cost (\$)	9106	8902	8781	8675	8583
ξ_1/ξ_2 (kW)	73/441	66/283	61/272	45/286	33/278
Average voltage satisfaction rate (%)	89.41	91.03	94.72	99.78	100
Computation time (min/day)	/	30.6	30.6	1.9	/

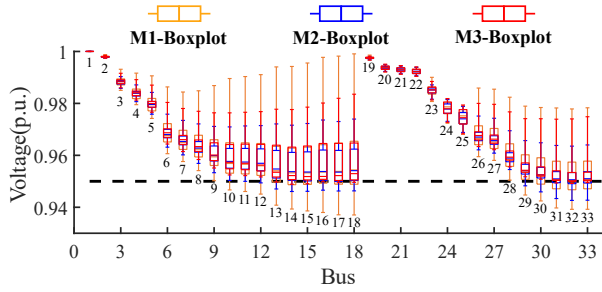


Fig. 5. Comparison of voltage distribution between M1-M3.

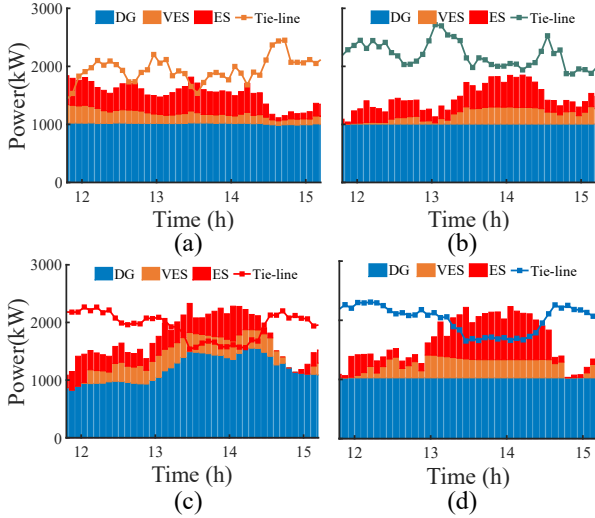


Fig. 6. Comparison of power dispatch (12h-15h) between (a) M1, (b) M2, (c) M3 and (d) M4.

(2) In terms of voltage satisfaction rate, M3 demonstrate a satisfactory rate. This is because the OCO algorithm can utilize the latest power data for online correction based on reference, thereby ensuring the secure operation of MG. However, owing to uncertainties or inaccuracies of predictions, M1-M2 sometimes fail to respond quickly to changes of RES. The imbalance power is then absorbed by the external grid, which can easily lead to voltage exceedances at nodes far from PCC, as shown in Fig. 5, posing a potential threat to the safe operation of MG. We found that prediction errors significantly influence the voltage satisfaction rate of M2, as well as the operation cost. In contrast, M3, which employs real-time control based on the latest data, effectively addresses this challenge.

(3) In terms of computation time, M3 calculate much faster than M2. This is because the reference update takes almost no computation time. The core step of OCO, (25), only needs to solve an approximately unconstrained optimization problem, which is highly efficiently. In contrast, the predictive and optimization model of EMPC contain the system states over a certain future time interval, which makes the model much larger than that of OCO. Therefore, the computation speed of M3 makes it more suitable for online operation compared to M2.

C. Benefit From Data-Driven Coordinated Dispatch

To demonstrate the benefit from data-driven coordinated dispatch, we compare the results for the following variants of M3:

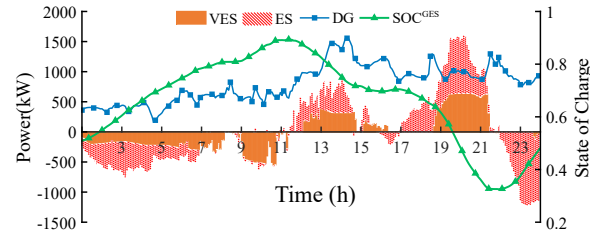


Fig. 7. 24-hour online power dispatch result of M3.

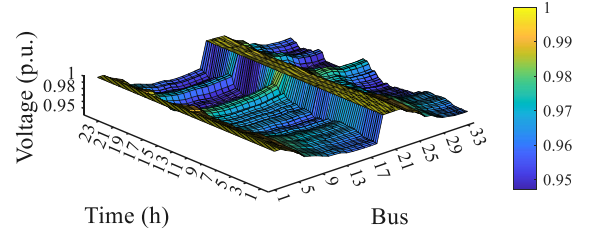


Fig. 8. The voltage profile of all buses of M3.

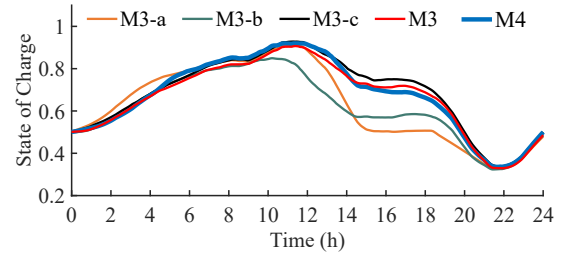


Fig. 9. Comparison of SoC^{GES} between different variants of M3 and M4.

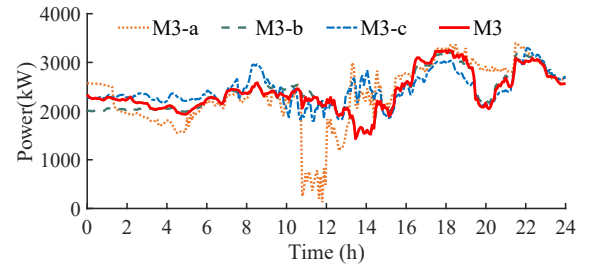


Fig. 10. Comparison of tie-line power between different variants of M3.

- 1) **M3-a**: online optimization with a greedy objective to minimize operating costs.
- 2) **M3-b**: the two-stage coordinated dispatch with a fixed reference—the average of ex-post optimal sequences.
- 3) **M3-c**: continuously updates the reference but strictly dispatches GES according to the reference.
- 4) **M3**: the proposed data-driven coordinated dispatch. The dispatch results over 68 days are compared in Table III.

TABLE III
COMPARISONS BETWEEN DIFFERENT VARIANTS OF M3 OVER 68 DAYS

Indices	M3-a	M3-b	M3-c	M3
Average operation cost (\$)	9038	8921	8817	8675
ξ_1/ξ_2 (kW)	96/501	37/340	62/311	45/286
Average voltage satisfaction rate (%)	96.17	99.03	96.92	99.78

For the typical scenario shown in Fig. 3(a), the results are presented in Figs. 7-10. M3-a, which lacks a “reference”, only cares about the instant costs, rapidly discharging when prices are high and likewise when prices are low. This leads to significant fluctuations in tie-line power and insufficient storage capacity during a sudden drop (13-15h) in the output of RES, resulting in high operation costs and low voltage satisfaction rate. The SOC and tie-line power curves of M3 are most closely aligned with those of M4. In contrast, M3-b exhibits significant differences when compared to M4. This is because M3 utilizes the latest uncertainty information to update the reference by sequentially adjusting the weights of historical scenarios as shown in Fig. 3(b). Consequently, it obtains reference with better suboptimality. M3-c operates the MG strictly according to the reference. However, due to the non-anticipativity, the fluctuations of RES are entirely absorbed by external grid, which not only leads to increased costs but also tends to cause voltage at the terminal nodes to go beyond the safe range. M3 addresses these shortcomings: the reference, based on historical experience, offers a global perspective with good sub-optimality, while the OCO algorithm provides real-time corrections. Consequently, M3 achieves both economical and secure operation of the MG.

D. Discussion

Due to factors such as communication delay, asynchronous communication, and measurement inaccuracy, the accuracy of real-time data affects the performance of the proposed method. We added a noise signal equivalent to $X\%$ of the real-time data to simulate inaccuracies, where $X \sim N(0, \sigma_c^2)$. The dispatch results under different noise signals are compared in Table IV. The voltage satisfaction rate is most affected, and the operational costs also increase with the rise in noise signals.

We have the weight parameters φ_1 and φ_2 in (23) to control how close to the reference. We conducted a sensitivity analysis on φ_1 and φ_2 . φ_1 and φ_2 have only a minor impact on the voltage satisfaction rate. Additionally, φ_1 has little effect on ξ_1 and ξ_2 . As in Fig. 12, selecting $\varphi_2 = 10^{-4}$ balances both cost and ξ_1/ξ_2 . As in Fig. 11, the cost first goes down and then goes up with φ_1 increasing. In this case, we have $\varphi_1 = 10^4$. Besides, we can use more samples of φ_1 and φ_2 to train a Pareto front for a better weight.

V. CONCLUSION

This paper proposes a data-driven, two-stage coordinated dispatch method for MG dispatch without prediction. Additionally, we propose a novel adaptive VQB online

TABLE IV
COMPARISON UNDER DIFFERENT NOISE SIGNALS.

Indices	$\sigma_c = \frac{10}{3}$	$\sigma_c = \frac{20}{3}$	$\sigma_c = \frac{30}{3}$	$\sigma_c = \frac{40}{3}$	$\sigma_c = \frac{50}{3}$
Operation cost(\$)	8716	8757	8792	8853	8894
ξ_1/ξ_2 (kW)	48/288	51/292	56/294	72/302	80/312
Voltage satisfaction rate (%)	96.85	94.42	92.57	91.31	90.77

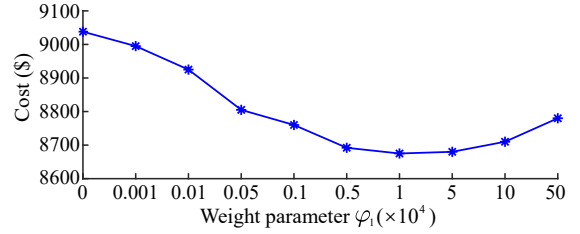


Fig. 11. Operation cost achieved by M3 with different φ_1 ($\varphi_2 = 10^{-4}$).

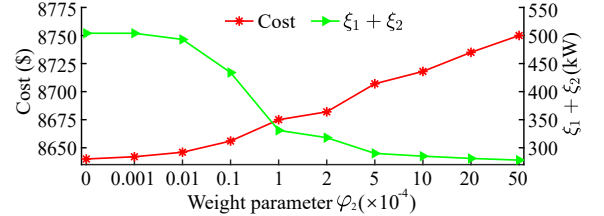


Fig. 12. Indices achieved by M3 with different φ_2 ($\varphi_1 = 10^4$).

optimization algorithm for MG based on the OCO framework. Simulation results verify that:

(1) The proposed method outperforms state-of-the-art methods and can nearly achieve the effect of the deterministic method with perfect knowledge of uncertainty, with operation cost differing by only 1.08%.

(2) Reference provides a global vision for the dispatch of GES, preventing myopic decisions during real-time operation. Moreover, reference update ensures better optimality and serves a role similar to prediction.

(3) The OCO algorithm can utilize the latest power data for online correction based on reference. It not only effectively mitigates rapid fluctuations of RES but also ensure the safe operation of MG, evidenced by a 99.78% voltage satisfaction rate. The computation speed of the proposed method is highly rapid, making it fully suitable for online applications.

Future work will focus on more complex operating conditions, such as OCO under weak communication conditions; market operation of MG; and the applications of OCO on distributed optimization of power system.

APPENDIX

A. Proof of the bound on dynamic regret

Let $\{x_{i,t}\} (\forall i \in \{1, 2, \dots, N\})$ and $\{x_t\}$ be the sequence generated by Algorithm1. Let $\{y_t\}$ be an arbitrary sequence in X . From f_t is convex and (31), we have

$$\begin{aligned}
 f_t(x_{i,t}) - f_t(y_t) &\leq \langle \partial f_t(x_{i,t}), x_{i,t} - y_t \rangle \\
 &\leq G \|x_{i,t} - x_{i,t+1}\| + \langle \partial f_t(x_{i,t}), x_{i,t+1} - y_t \rangle \\
 &\leq \frac{G^2 \alpha_{i,t}}{2} + \frac{1}{2\alpha_{i,t}} \|x_{i,t} - x_{i,t+1}\|^2 + \langle \partial f_t(x_{i,t}), x_{i,t+1} - y_t \rangle.
 \end{aligned} \tag{37}$$

For the third term of (37), we have

$$\begin{aligned}
 &\langle \partial f_t(x_{i,t}), x_{i,t+1} - y_t \rangle \\
 &= \langle \beta_{t+1}(Q_i(t) \circ \partial[g_t(x_{i,t+1})]_+), y_t - x_{i,t+1} \rangle \\
 &+ \langle \partial f_t(x_{i,t}) + \beta_{t+1}(Q_i(t) \circ \partial[g_t(x_{i,t+1})]_+), x_{i,t+1} - y_t \rangle.
 \end{aligned} \tag{38}$$

It is trivial that $[g_t]_+$ is convex. We have

$$\begin{aligned} & \langle \beta_{t+1}(Q_i(t) \circ \partial[g_t(x_{i,t+1})]_+), y_t - x_{i,t+1} \rangle \\ & \leq \beta_{t+1} \langle Q_i(t), [g_t(y_t)]_+ \rangle - \beta_{t+1} \langle Q_i(t), [g_t(x_{i,t+1})]_+ \rangle. \end{aligned} \quad (39)$$

Note that (25) can be written in the following form:

$$x_{i,t+1} = \operatorname{argmin}_{x \in X} \{h(x) + \|x - x_{i,t}\|^2\}. \quad (40)$$

From Lemma 1 in reference [32], we have:

$$\begin{aligned} & \langle \partial f_t(x_{i,t}) + \beta_{t+1}(Q_i(t) \circ \partial[g_t(x_{i,t+1})]_+), x_{i,t+1} - y_t \rangle \\ & \leq \frac{1}{\alpha_{i,t}} (\|y_t - x_{i,t}\|^2 - \|y_t - x_{i,t+1}\|^2 - \|x_{i,t+1} - x_{i,t}\|^2). \end{aligned} \quad (41)$$

Combining (37), (38), (39) and (41) gives

$$\begin{aligned} f_t(x_{i,t}) - f_t(y_t) & \leq \frac{G^2 \alpha_{i,t}}{2} + \frac{1}{\alpha_{i,t}} (\|y_t - x_{i,t}\|^2 - \|y_t - x_{i,t+1}\|^2) \\ & \quad + \beta_{t+1} \langle Q_i(t), [g_t(y_t)]_+ \rangle. \end{aligned} \quad (42)$$

Let the optimal sequence be $\{x_t^*\}$. Substitute $\{y_t\} = \{x_t^*\}$ in (42). Note that $g_t(x_t^*) \leq 0$ because $\mathcal{X}_t^* \in X$, which gives

$$\begin{aligned} & \sum_{t=1}^T f_t(x_{i,t}) - \sum_{t=1}^T f_t(x_t^*) \\ & \leq \sum_{t=1}^T \frac{1}{\alpha_{i,t}} (\|x_t^* - x_{i,t}\|^2 - \|x_t^* - x_{i,t+1}\|^2) + \sum_{t=1}^T \frac{G^2 \alpha_{i,t}}{2}. \end{aligned} \quad (43)$$

Using (29) and (32) yields

$$\begin{aligned} & \sum_{t=1}^T \frac{1}{\alpha_{i,t}} (\|x_t^* - x_{i,t}\|^2 - \|x_t^* - x_{i,t+1}\|^2) \\ & \leq \frac{1}{2^{i-1}} ((d(X))^2 (T+1)^{\frac{1}{2}+\chi} + 2d(X)P_x T^{\frac{1}{2}+\chi}). \end{aligned} \quad (44)$$

For the second term of (43), we have

$$\sum_{t=1}^T \frac{G^2 \alpha_{i,t}}{2} \leq \frac{2^{i-1} G^2}{2} \sum_{t=1}^T \frac{1}{t^{\frac{1}{2}+\chi}} \leq \frac{2^{i-1} G^2}{1-2\chi} T^{\frac{1}{2}-\chi}. \quad (45)$$

Combining (43)-(45) gives

$$\begin{aligned} \sum_{t=1}^T f_t(x_{i,t}) - \sum_{t=1}^T f_t(x_t^*) & \leq \frac{2}{2^{i-1}} ((d(X))^2 T^{\frac{1}{2}+\chi} (1 + \frac{P_x}{d(X)}) \\ & \quad + \frac{2^{i-1} G^2}{1-2\chi} T^{\frac{1}{2}-\chi}). \end{aligned} \quad (46)$$

Let $i_0 = \lceil \frac{1}{2} \log_2(1 + \frac{P_x}{d(X)}) \rceil + 1 \in [N]$ such that

$$2^{i_0-1} \leq \sqrt{1 + \frac{P_x}{d(X)}} \leq 2^{i_0}. \quad (47)$$

Substitute i_0 in (46), and combining (46) and (47) yield

$$\sum_{t=1}^T f_t(x_{i_0,t}) - \sum_{t=1}^T f_t(x_t^*) \leq (4(d(X))^2 + \frac{G^2}{1-2\chi}) T^{\frac{1}{2}+\chi} \sqrt{1 + \frac{P_x}{d(X)}} \leq \frac{\alpha_{i_0,t}^2 G^2}{4} + \alpha_{i_0,t} |f_t(x_{i_0,t}) - f_t(x_t^*)| + \|x_t^* - x_{i_0,t}\|^2 - \|x_t^* - x_{i_0,t+1}\|^2. \quad (48)$$

From (28) and that f_t is convex, we have

$$f_t(x_t) - f_t(x_{i_0,t}) \leq l_t(x_t) - l_t(x_{i_0,t}). \quad (49)$$

Applying Lemma 1 in reference [29] to (27) and (28) yields

$$\sum_{t=1}^T l_t(x_t) - \min_{i \in [N]} \left\{ \sum_{t=1}^T l_t(x_{i,t}) + \frac{1}{\gamma} \ln \frac{1}{\rho_{i,1}} \right\} \leq \frac{\gamma (Gd(X))^2 T}{2}. \quad (50)$$

$$\sum_{t=1}^T f_t(x_t) - \sum_{t=1}^T f_t(x_{i_0,t}) \leq \frac{(Gd(X))^2 \sqrt{T}}{2} + \sqrt{T} \ln \frac{1}{\rho_{i_0,1}}. \quad (51)$$

From $\rho_{i,1} = (N+1)/[i(i+1)N]$, we have

$$\ln \frac{1}{\rho_{i_0,1}} \leq \ln(i_0(i_0+1)) \leq 2\ln(i_0+1) \leq 2\ln\left(\left[\frac{1}{2} \log_2\left(1 + \frac{P_x}{d(X)}\right)\right] + 1\right). \quad (52)$$

Combining (48), (51) and (52) yields (33).

B. Proof of the bound on cumulative constraint violations

Define

$$\begin{aligned} p_t(x) & := \alpha_{i,t} \langle \partial f_t(x_{i,t}), x - x_{i,t} \rangle \\ & \quad + \alpha_{i,t} \beta_t \langle Q_i(t), [g_t(x)]_+ \rangle + \|x - x_{i,t}\|^2. \end{aligned} \quad (53)$$

Note that $p_t(x)$ and $\|x - x_t\|^2$ are 2-strongly convex, which gives

$$p(x) \geq p(y) + \langle \partial p(y), x - y \rangle + \|x - y\|^2. \quad (54)$$

According to (25), we have $x_{i,t+1} = \operatorname{argmin}_{x \in X} p(x)$. Based on the first-order optimality condition, we have

$$\langle \partial p(x_{i,t+1}), x - x_{i,t+1} \rangle \geq 0. \quad (55)$$

Substitute $y = x_{i,t+1}$ and $x = x_t^*$ in (54), and combining (53)-(55) yields

$$\begin{aligned} & \alpha_{i,t} \langle \partial f_t(x_{i,t}), x_{i,t+1} - x_{i,t} \rangle + \alpha_{i,t} \beta_t \langle Q_i(t), [g_t(x_{i,t+1})]_+ \rangle \\ & \quad + \|x_{i,t+1} - x_{i,t}\|^2 \\ & \leq \alpha_{i,t} \langle \partial f_t(x_{i,t}), x_t^* - x_{i,t} \rangle + \alpha_{i,t} \beta_t \langle Q_i(t), [g_t(x_t^*)]_+ \rangle \\ & \quad + \|x_t^* - x_{i,t}\|^2 - \|x_t^* - x_{i,t+1}\|^2. \end{aligned} \quad (56)$$

We add $\alpha_{i,t} f_t(x_{i,t})$ to both sides and rearranging terms:

$$\begin{aligned} & \alpha_{i,t} f_t(x_{i,t}) - \alpha_{i,t} (f_t(x_{i,t}) + \langle \partial f_t(x_{i,t}), x_t^* - x_{i,t} \rangle) \\ & \quad + \alpha_{i,t} \beta_t \langle Q_i(t), [g_t(x_{i,t+1})]_+ \rangle \\ & \leq \alpha_{i,t} \langle \partial f_t(x_{i,t}), x_{i,t} - x_{i,t+1} \rangle + \alpha_{i,t} \beta_t \langle Q_i(t), [g_t(x_t^*)]_+ \rangle \\ & \quad - \|x_{i,t+1} - x_{i,t}\|^2 + \|x_t^* - x_{i,t}\|^2 - \|x_t^* - x_{i,t+1}\|^2. \end{aligned} \quad (57)$$

From $[g_t(x_t^*)]_+ = 0$, combining (31) and (57) yields

$$\begin{aligned} & \alpha_{i,t} f_t(x_{i,t}) - \alpha_{i,t} f_t(x_t^*) + \alpha_{i,t} \beta_t \langle Q_i(t), [g_t(x_{i,t+1})]_+ \rangle \\ & \leq \frac{\alpha_{i,t}^2 G^2}{4} + \|x_t^* - x_{i,t}\|^2 - \|x_t^* - x_{i,t+1}\|^2. \end{aligned} \quad (58)$$

From (58), we have

$$\begin{aligned} & \alpha_{i,t} \beta_t \langle Q_i(t), [g_t(x_{i,t+1})]_+ \rangle \\ & \leq \frac{\alpha_{i,t}^2 G^2}{4} + \alpha_{i,t} |f_t(x_{i,t}) - f_t(x_t^*)| + \|x_t^* - x_{i,t}\|^2 - \|x_t^* - x_{i,t+1}\|^2. \end{aligned} \quad (59)$$

From (26), we have

$$\alpha_{i,t} \beta_t \langle Q_i(t), [g_t(x_{i,t+1})]_+ \rangle \geq \alpha_{i,t} \beta_t \theta_{i,t} \| [g_t(x_{i,t+1})]_+ \|_1; \quad (60)$$

Combining (32), (59) and (60) yields

$$\begin{aligned} \|[g_t(x_{i,t+1})]_+\|_1 &\leq \frac{G^2}{4t^{2+\delta+\chi}} + \frac{|f_t(x_{i,t}) - f_t(x_t^*)|}{2^{i-1}t^{\frac{3}{2}+\delta}} \\ &\quad + \frac{\|x_t^* - x_{i,t}\|^2 - \|x_t^* - x_{i,t+1}\|^2}{4^{i-1}t^{1+\delta-\chi}}. \end{aligned} \quad (61)$$

Under Assumptions 1-3, summing (61) over $t \in \{1, \dots, T\}$ yields

$$\sum_{t=1}^T \|[g_t(x_{i,t+1})]_+\|_1 \leq \frac{G^2}{2} + \frac{3F}{2^{i-1}} + \left(1 + \frac{1}{\delta-\chi}\right) \frac{(d(X))^2}{4^{i-1}}. \quad (62)$$

From Cauchy-Schwarz inequality, we have

$$\begin{aligned} \|[g_t(x_{i,t})]_+\|_1 - \|[g_t(x_{i,t+1})]_+\|_1 \\ \leq \|\partial [g_t(x_{i,t})]_+\| \|x_{i,t} - x_{i,t+1}\| \leq \frac{G^2}{4\eta} + \eta \|x_{i,t} - x_{i,t+1}\|^2, \end{aligned} \quad (63)$$

where $\eta = T^{\chi/2}$. Summing (63) over $t \in \{1, \dots, T\}$ yields

$$\begin{aligned} \sum_{t=1}^T \|[g_t(x_{i,t})]_+\|_1 - \|[g_t(x_{i,t+1})]_+\|_1 \\ \leq \frac{G^2}{4} T^{1-\frac{\chi}{2}} + 2^{i-1} (F + Gd(X)) \frac{2}{1-2\chi} T^{\frac{1}{2}-\frac{\chi}{2}} + (d(X))^2 T^{\frac{\chi}{2}} \end{aligned} \quad (64)$$

Combining (62) and (64) yields

$$\begin{aligned} \sum_{t=1}^T \|[g_t(x_{i,t})]_+\|_1 &\leq \frac{G^2}{2} + 3\frac{F}{2^{i-1}} + \left(1 + \frac{1}{\delta-\chi}\right) \frac{(d(X))^2}{4^{i-1}} \\ &\quad + (d(X))^2 T^{\frac{\chi}{2}} + \left(\frac{G^2}{4} T^{1-\frac{\chi}{2}} + 2^{i-1} (F + Gd(X))\right) \frac{2}{1-2\chi} T^{\frac{1}{2}-\frac{\chi}{2}} \end{aligned} \quad (65)$$

Combining (27), (28), (32) and (65) yields (34).

REFERENCES

- [1] H. Qiu, W. Gu, X. Xu *et al.*, "A historical-correlation-driven robust optimization approach for microgrid dispatch," *IEEE Trans. Smart Grid*, vol. 12, no. 2, pp. 1135–1148, 2021.
- [2] K. Antoniadou-Plytaria, D. Steen, O. Carlson *et al.*, "Scenario-based stochastic optimization for energy and flexibility dispatch of a microgrid," *IEEE Trans. Smart Grid*, vol. 13, no. 5, pp. 3328–3341, 2022.
- [3] N. Qi, P. Pinson, M. R. Almassalkhi *et al.*, "Chance-constrained generic energy storage operations under decision-dependent uncertainty," *IEEE Trans. Sustain. Energy*, 2023.
- [4] Z. Li and Y. Xu, "Temporally-coordinated optimal operation of a multi-energy microgrid under diverse uncertainties," *Appl. Energy*, vol. 240, pp. 719–729, 2019.
- [5] J. Hu, Y. Shan, Y. Yang *et al.*, "Economic model predictive control for microgrid optimization: A review," *IEEE Trans. Smart Grid*, 2023.
- [6] Z. Li, L. Wu, Y. Xu *et al.*, "Multi-stage real-time operation of a multi-energy microgrid with electrical and thermal energy storage assets: A data-driven mpc-adp approach," *IEEE Trans. Smart Grid*, vol. 13, no. 1, pp. 213–226, 2021.
- [7] C. Hu, Z. Cai, Y. Zhang *et al.*, "A soft actor-critic deep reinforcement learning method for multi-timescale coordinated operation of microgrids," *Prot. Control Mod. Power Syst.*, vol. 7, no. 1, p. 29, 2022.
- [8] M. Zhang, Z. Zhen, N. Liu *et al.*, "Optimal graph structure based short-term solar pv power forecasting method considering surrounding spatio-temporal correlations," *IEEE Trans. Ind. Appl.*, vol. 59, no. 1, pp. 345–357, 2022.
- [9] E. Sarmas, E. Spiliotis, E. Stamatopoulos *et al.*, "Short-term photovoltaic power forecasting using meta-learning and numerical weather prediction independent long short-term memory models," *Renewable Energy*, vol. 216, p. 118997, 2023.
- [10] Z. Wang, W. Wei, J. Z. F. Pang *et al.*, "Online optimization in power systems with high penetration of renewable generation: Advances and prospects," *IEEE/CAA J. Autom. Sinica*, vol. 10, no. 4, pp. 839–858, 2023.
- [11] S.-J. Kim and G. B. Giannakis, "An online convex optimization approach to real-time energy pricing for demand response," *IEEE Trans. Smart Grid*, vol. 8, no. 6, pp. 2784–2793, 2017.
- [12] T. Zhao, A. Parisio, and J. V. Milanović, "Distributed control of battery energy storage systems for improved frequency regulation," *IEEE Trans. Power Syst.*, vol. 35, no. 5, pp. 3729–3738, 2020.
- [13] A. Lesage-Landry, H. Wang, I. Shames *et al.*, "Online convex optimization of multi-energy building-to-grid ancillary services," *IEEE Trans. Control Syst. Technol.*, vol. 28, no. 6, pp. 2416–2431, 2020.
- [14] X. Ding, L. Chen, P. Zhou *et al.*, "Dynamic online convex optimization with long-term constraints via virtual queue," *Inf. Sci.*, vol. 577, pp. 140–161, 2021.
- [15] H. Yu and M. J. Neely, "A low complexity algorithm with $o(\sqrt{T})$ regret and $o(1)$ constraint violations for online convex optimization with long term constraints," *J. Mach. Learn. Res.*, vol. 21, no. 1, pp. 1–24, 2020.
- [16] Q. Liu, W. Wu, L. Huang *et al.*, "Simultaneously achieving sublinear regret and constraint violations for online convex optimization with time-varying constraints," *Perform. Evaluation Rev.*, vol. 49, no. 3, pp. 4–5, 2022.
- [17] X. Yi, X. Li, T. Yang *et al.*, "Regret and cumulative constraint violation analysis for online convex optimization with long term constraints," in *Proc. Int. Conf. Mach. Learn.* PMLR, 2021, pp. 11998–12008.
- [18] X. Cao, J. Zhang, and H. V. Poor, "Constrained online convex optimization with feedback delays," *IEEE Trans. Autom. Control*, vol. 66, no. 11, pp. 5049–5064, 2021.
- [19] D. Muthirayan, J. Yuan, and P. P. Khargonekar, "Online convex optimization with long-term constraints for predictable sequences," *IEEE Control Syst. Lett.*, vol. 7, pp. 979–984, 2023.
- [20] X. Yi, X. Li, T. Yang *et al.*, "Regret and cumulative constraint violation analysis for distributed online constrained convex optimization," *IEEE Trans. Autom. Control*, 2022.
- [21] A. Niromandfam, A. M. Pour, and E. Zarezaeh, "Virtual energy storage modeling based on electricity customers' behavior to maximize wind profit," *J. Energy Storage*, vol. 32, p. 101811, 2020.
- [22] Y. Ding, D. Xie, H. Hui *et al.*, "Game-theoretic demand side management of thermostatically controlled loads for smoothing tie-line power of microgrids," *IEEE Trans. Power Syst.*, vol. 36, no. 5, pp. 4089–4101, 2021.
- [23] Z. Li, Q. Guo, H. Sun *et al.*, "Sufficient conditions for exact relaxation of complementarity constraints for storage-concerned economic dispatch," *IEEE Trans. Power Syst.*, vol. 31, no. 2, pp. 1653–1654, 2016.
- [24] N. Qi, L. Cheng, H. Xu *et al.*, "Smart meter data-driven evaluation of operational demand response potential of residential air conditioning loads," *Appl. Energy*, vol. 279, p. 115708, 2020.
- [25] K. Baker and A. Bernstein, "Joint chance constraints in ac optimal power flow: Improving bounds through learning," *IEEE Trans. Smart Grid*, vol. 10, no. 6, pp. 6376–6385, 2019.
- [26] M. Vrakopoulou, B. Li, and J. L. Mathieu, "Chance constrained reserve scheduling using uncertain controllable loads part i: Formulation and scenario-based analysis," *IEEE Trans. Smart Grid*, vol. 10, no. 2, pp. 1608–1617, 2019.
- [27] T. Homem-de Mello and G. Bayraksan, "Monte carlo sampling-based methods for stochastic optimization," *Surveys in Operations Research and Management Science*, vol. 19, no. 1, pp. 56–85, 2014.
- [28] H. J. Bierens, "The nadaraya-watson kernel regression function estimator," 1988.
- [29] L. Zhang, S. Lu, and Z.-H. Zhou, "Adaptive online learning in dynamic environments," *Proc. Adv. Neural Inf. Process. Syst.*, vol. 31, 2018.
- [30] Z. Wang, B. Chen, J. Wang *et al.*, "Robust optimization based optimal dg placement in microgrids," *IEEE Trans. Smart Grid*, vol. 5, no. 5, pp. 2173–2182, 2014.
- [31] W. Su, J. Wang, and J. Roh, "Stochastic energy scheduling in microgrids with intermittent renewable energy resources," *IEEE Trans. Smart Grid*, vol. 5, no. 4, pp. 1876–1883, 2014.
- [32] X. Yi, X. Li, L. Xie *et al.*, "Distributed online convex optimization with time-varying coupled inequality constraints," *IEEE Trans. Signal Process.*, vol. 68, pp. 731–746, 2020.